INRIA

Wall-Laws for High Speed Flows over Adiabatic and Isothermal Walls

Bijan Mohammadi and Guillaume Puigt

No 3948

May 2000

———— THÈME 4 ————

*R apport
de recherche*

Wall-Laws for High Speed Flows over Adiabatic and Isothermal Walls

Bijan Mohammadi [*] and Guillaume Puigt [†]

Thème 4 — Simulation et optimisation
de systèmes complexes

Projet M3N

Abstract: We present the extension of our wall-laws developed for low-speed flows to super and hypersonic configurations. In particular, we are interested in flows over isothermal walls and account for heat transfer. We recall the main steps of the development:

- Obtaining generalized wall functions for low-speed fluids, valid for all y^+,
- Taking into account transversal effects.
- Accounting for the compressible feature of the flow on adiabatic walls without using informations on the local boundary layer structure but only those available at the fictitious wall.
- Extension to isothermal walls. A posteriori evaluation of the heat flux at the real wall using informations at the fictitious one.
- Only use informations available on unstructured meshes and avoid those coming from a Cartesian hypothesis for the mesh in near-wall regions.

These ingredients are validated on hypersonic configurations on adiabatic and isothermal walls for expansion and compression ramps as well as for reentry geometries.

Key-words: Generalized wall-laws, Crocco relation, Reynolds relation, adiabatic, isothermal.

(Résumé : tsvp)

[*] e-mail: Bijan.Mohammadi@inria.fr
[†] e-mail: puigt@math.univ-montp2.fr

Lois de Paroi pour Ecoulements à Grande Vitesse sur Parois Adiabatiques et Isothermes

Résumé : Ce travail concerne l'extension des lois de paroi généralisées développées jusque là pour les écoulements à faible vitesse aux configurations super et hypersoniques. De plus, on s'intéresse aux transferts thermiques et à la modélisation des parois isothermes. On rappelle les étapes principales du développement:

- Obtention des lois généralisées pour les fluides incompressibles valable pour tout y^+.
- Prise en compte des effets transverses.
- Prise en compte de l'aspect compressible des flots pour parois adiabatiques, cette prise en compte ne devant pas nécessiter la connaissance a priori de l'épaisseur locale de la couche limite mais uniquement des variables à la paroi fictive de calcul.
- Prise en compte des échanges thermiques sur parois isothermes. En particulier, on accéde aux flux thermiques à la paroi réelle par une évaluation a posteriori en utilisant l'information calculée sur la paroi fictive.
- Utilisation uniquement des informations disponibles en maillage non-structuré : on évite celles utilisant une hypothèse a priori sur l'orthogonalité des mailles à la paroi.

Ces ingrédients ont été validés sur des configurations hypersoniques sur parois adiabatiques puis isothermes, notamment de rampes de détente et de compression et sur des corps de rentrée.

Mots-clé : Lois de paroi généralisées, relation de Crocco, relation de Reynolds, adiabatique, isotherme.

Contents

11 Concluding remarks   **20**

12 Appendix 1: Generating Inflow Profiles   **28**

**13 Appendix 2: The Chien $k - \varepsilon$ turbulence model**   **29**

1   Introduction

The general idea in wall-laws is to remove the stiff part from boundary layers, replacing the classical no-slip boundary condition by a more sophisticated relation between the variables and their derivatives [1]. In the past, we have developed a global strategy for boundary layer computations using this idea. We showed that the approach is enough general for the simulation of separated and unsteady flows for incompressible and weakly compressible fluids and leads to good agreement with experiments [2, 3].

The aim of this paper is to present the generalization of our wall functions formulation and implementation for high speed separated flows on adiabatic and isothermal walls. The turbulence modeling is done using either a two-layer $k - \varepsilon$ model [4, 5, 6] to account for low-Reynolds regions existing in separated flows or a high-Reynolds $k - \varepsilon$ coupled with the wall functions presented here. The aim is to recover by the former approach what obtained with the first one. As a consequence, the motivation is to predict the fluxes at the real wall thanks to informations coming from the fictitious one: we do not take into account the region stated between them, and that contains most of the physics of the flow.

The particular ingredients of our wall functions implementation are:

1. Global wall-laws in y^+ : valid up to the wall.
2. Weak formulation: this permits to easily take pressure effects into account in the boundary integrals.
3. Small δ in wall-laws: this means that the computational domain should not be too far from the wall.
4. Fine meshes: the computational mesh should be fine enough so that the numerical results become mesh independent. Something which has not been always satisfied when using wall- laws.
5. Global wall-laws in Mach number: to account for compressibility effects.
6. Temperature dependence: to account for both adiabatic and isothermal walls.
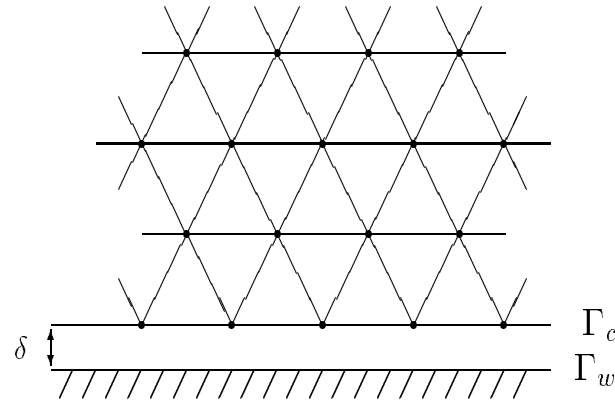
Γ_c is the fictitious computational wall whereas Γ_w is the real wall. In practice, we have $\Gamma_c = \Gamma_w$ and we use the same mesh, the effective Reynolds number is therefore $Re' = Re \frac{L+\delta}{L}$.

Another motivation for the development of wall-laws is that we are interested by an approach which avoids the need for the distance to the wall in turbulence models. This is why we use the wall functions with the high-Reynolds version of the turbulence models. This is important for parallel computation, especially when targeting moving domain on multi-body configurations simulation on distributed platform (using an ALE approach for instance). The question arises also in shape optimization where after shape and mesh deformation we need to recover the distance to the wall [7, 8, 9]. Another motivation comes from the industrial needs for simulations over rough boundaries. Indeed, this wall function approach has been extended in the past for low-speed flows [10, 11] over rough surfaces and we are today targeting a similar extension for high-speed configurations. A last point of importance is that wall functions coupled with RANS models for near-wall regions seem to be a realistic way to provide near-wall treatment and boundary conditions for LES simulations.

2   Governing Equations

Consider the non-dimensionalized Navier-Stokes system in conservation variables. We split the variables into mean and fluctuating parts. We use a Reynolds average for the density and pressure and a Favre average for the other variables [12]. Following [12] for the modeling, this leads to the Reynolds averaged Navier-Stokes equations:

$$\frac{\partial \rho}{\partial t} + \nabla \cdot (\rho u) = 0 \,,$$

$$\frac{\partial \rho u}{\partial t} + \nabla \cdot (\rho u \otimes u) + \nabla p = \nabla \cdot ((\mu + \mu_t)S) \,, \tag{1}$$

$$\frac{\partial \rho E}{\partial t} + \nabla \cdot ((\rho E + p)u) = \nabla \cdot ((\mu + \mu_t)Su) + \nabla((\chi + \chi_t)\nabla T) \,,$$

with

$$\chi = \frac{\gamma \mu}{Pr}, \quad \chi_t = \frac{\gamma \mu_t}{Pr_t},$$

$$\gamma = 1.4, \quad Pr = 0.72 \quad \text{and} \quad Pr_t = 0.9 \,.$$

μ and μ_t are the inverse of the laminar and turbulent Reynolds numbers. In what follows, we call them viscosity. The laminar viscosity μ is given by Sutherland law:

$$\mu = \mu_\infty (\frac{T}{T_\infty})^{1.5} (\frac{T_\infty + 110.4}{T + 110.4}), \tag{2}$$

where ∞ denotes reference quantities.

We do not take into account the turbulent kinetic energy contribution to the pressure and total energy and keep the usual laws for a perfect gas [1].

2.1 Turbulence modeling

To close the previous system, we use two low-Reynolds versions of the Chien $k - \varepsilon$ model [13, 5, 1, 6]: the classical Chien model which is shortly described in appendix 2 and a two-layer reduction of the model which has shown more numerical robustness. We introduce Y_L, a maximum limit where the low-Reynolds model is applied. This is to avoid numerical problems when starting from uniform flows which leads to small y^+.

In high-Reynolds regions $Y^+ > 200$ or $y > Y_L$

$$\frac{\partial \rho k}{\partial t} + \nabla.(\rho u k) - \nabla((\mu + \mu_t)\nabla k) = S_k, \tag{3}$$

and

$$\frac{\partial \rho \varepsilon}{\partial t} + \nabla.(\rho u \varepsilon) - \nabla((\mu + c_\varepsilon \mu_t)\nabla \varepsilon) = S_\varepsilon. \tag{4}$$

The right hand sides of (3)-(4) contain the production and the destruction terms for ρk and $\rho \varepsilon$:

$$S_k = \mu_t P - \frac{2}{3}\rho k \nabla.u - \rho \varepsilon, \tag{5}$$

$$S_\varepsilon = c_1 \rho k P - \frac{2c_1}{3c_\mu}\rho \varepsilon \nabla.u - c_2 \rho \frac{\varepsilon^2}{k}. \tag{6}$$

The eddy viscosity is given by:

$$\mu_t = c_\mu \rho \frac{k^2}{\varepsilon}. \tag{7}$$

The constants $c_\mu, c_1, c_2, c_\varepsilon$ are respectively $0.09, 0.1296, 11/6, 1/1.4245$ and $P = S : \nabla u$. The constant c_2 and c_ε are different from their original values of 1.92 and 1/1.3 but this is more in agreement with recent experiences [14, 15].

In Low-Reynolds regions $y^+ < 200$ and $y < Y_L$

The eddy viscosity is given by:

$$\mu_t = c_\mu \rho \sqrt{k} l_\mu \,, \text{ with } l_\mu = \kappa c_\mu^{-3/4} y \left(1 - exp(\frac{-y^+}{0.0142})\right).$$

The right hand side of k equation comes from the Chien model:

$$S_k = \mu_t P - \frac{2}{3}\rho k \nabla.u - \rho \varepsilon - 2\mu \frac{k}{y^2} \,.$$

and ε is deduced from:

$$\varepsilon = \frac{k^{3/2}}{l_\varepsilon}, \ \text{ with } l_\varepsilon = \kappa c_\mu^{-3/4} y \left(1 - exp(\frac{-y^+}{2\kappa c_\mu^{-3/4}}) \right) . \tag{8}$$

Remark:

One interesting feature of this two-layer formulation is that it enables for the analysis of the low-Reynolds behavior of the model and the impact of coupling later the full model or only its high-Reynolds part with wall functions. Of course, we are interested by the former choice as said before.

3   Boundary and Initial Conditions

Inflow and outflow: inflow and outflow boundary conditions are of characteristic types where we impose the value of a variable if the corresponding wave is entering the domain (following the sign of the eigenvalue of the system). A Stegger-Warming [16] flux splitting scheme is used for in and outflow boundaries.

Symmetry: slipping boundary condition is imposed in weak form for these boundaries.

$$u.n = 0, \ \frac{\partial}{\partial n}(u.t) = 0, \ \frac{\partial k}{\partial n} = 0 \text{ and } \frac{\partial \varepsilon}{\partial n} = 0.$$

Solid walls: The classical boundary condition is no-slip boundary condition for the velocity ($u = 0$) and for the temperature, according to the physics of the problem, either adiabatic ($\frac{\partial T}{\partial n} = 0$) or isothermal ($T = T_{given}$) condition, $k = 0$ and $\varepsilon = 0$ for the two-layer formulation of the Chien model above.

When using wall functions, we remove part of the near-wall region and replace the previous conditions by Fourier type conditions: $u_\delta.n = f_1(\frac{\partial u_\delta}{\partial n}, \frac{\partial T_\delta}{\partial n})$ and $T_\delta = f_2(\frac{\partial u_\delta}{\partial n}, \frac{\partial T_\delta}{\partial n})$ for isothermal walls. Our aim through this paper is the description of this point.

Initial conditions: The initial flow is taken to be uniform with small values for k and ε.

4   Numerics

The spatial discretization of the Navier-Stokes equations is based on a Finite-Volume-Galerkin formulation. In this paper we use a Roe [17] Riemann solver for the convective part of the equations together with MUSCL reconstruction with Van Albada [18] type

limiters. The viscous terms are treated using a Galerkin Finite Element method on linear triangular elements.

We give a brief description of this technique applied to (1). Consider the following form of the Navier-Stokes equations:

$$\frac{\partial W}{\partial t} + \nabla.(F(W) - N(W, \nabla W)) = S(W, \nabla W), \tag{9}$$

where $W = (\rho, \rho u, \rho v, \rho E, \rho k, \rho \varepsilon)^t$ is the vector of conservation variables, F and N are the convective and diffusive operators. $S = (0, 0, 0, 0, S_k, S_\varepsilon)^t$ accounts for the turbulence model right hand sides.

Let $\Omega_h = \cup_j T_j$ be a discretization by triangles of the computational domain Ω and let $\Omega_h = \cup_i C_i$ be its partition in cells.
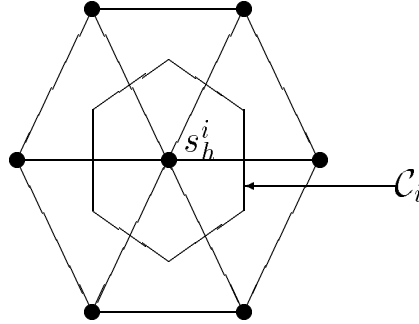
Thus, we can associate to each $w_h \in V_h$, where V_h is the set of the continuous affine functions on our triangulation, a w_h' piecewise constant function on cells by

$$w_h'|C_i = \frac{1}{|C_i|} \int_{C_i} w_h.$$

Conversely, knowing w_h' piecewise constant, w_h is obtained as $w_h(s_i^h) = w_h'|C_i$

The weak formulation of (9) is:

Find $W_h \in (V_h)^6$ such that, $\forall \phi_h \in V_h$

$$\int_{\Omega_h} \frac{\partial W_h}{\partial t} \phi_h - \int_{\Omega_h} (F_h - N_h)(W_h, \nabla W_h) \nabla (\phi_h) \tag{10}$$

$$+ \int_{\partial \Omega_h} (F_h - N_h) \cdot n \phi_h = \int_{\Omega_h} S_h(W_h, \nabla W_h) \phi_h.$$

This is equivalent to the following weak formulation obtained by taking in the convective part of (10) for ϕ_h the characteristic function of C_i and by using an explicit time integration:

$$|C_i|(\frac{W_i^{n+1} - W_i^n}{\Delta t}) + \int_{\partial C_i} F_d(W^n) \cdot n = R.H.S. \tag{11}$$

We use a centered scheme to compute the right hand side:

$$R.H.S. = -\int_{\Omega_h} N(W^n)\nabla(\phi_h) + \int_{\partial \Omega_h} N(W^n) \cdot n\phi_h + \int_{\Omega_h} S_h(W_h, \nabla W_h)\phi_h.$$

We show below how the boundary integral above accounts for wall functions in weak form. Moreover, $F_d(W_h^n) = F(W_{\partial \Omega_h})$ on $\partial C_i \cap \partial \Omega_h$ and elsewhere F_d is a piecewise constant upwinded approximation of $F(W)$ satisfying

$$\int_{\partial C_i} F_d \cdot n = \sum_{j \neq i} \Phi(W'|_{C_i}, W'|_{C_j}) \int_{\partial C_i \cap C_j} n. \tag{12}$$

After, writing $\tilde{B}$ for the jacobian of F at Roe's mean values, we take for Φ the Roe flux

$$\Phi_{Roe}(u, v) = \frac{1}{2}(F(u) + F(v)) - |\tilde{B}|\frac{(v - u)}{2}.$$

Spatial second order accuracy is obtained by using a MUSCL like extension involving a combinations of upwind and centered gradients. More precisely, let ∇W_i be an approximation of the gradient of W at node i. We define the following quantities on the segment $[i, j]$

$$W_{ij} = W_i + 0.5\text{Lim}(\beta(\nabla W)_i \vec{ij}, (1 - \beta)(W_i - W_j)),$$

and

$$W_{ji} = W_j - 0.5\text{Lim}(\beta(\nabla W)_j \vec{ij}, (1 - \beta)(W_j - W_i)),$$

with Lim being a Van Albada type limiter [18]:

$$\text{Lim}(a, b) = 0.5(1 + sgn(ab))\frac{(a^2 + \alpha)b + (b^2 + \alpha)a}{a^2 + b^2 + 2\alpha}$$

with $0 < \alpha << 1$ and β a positive constant containing the amount of upwinding $\beta \in [0, 1]$ (here $\beta = 2/3$). Now, the second order accuracy in space is obtained by replacing $W'|_{C_i}$ and $W'|_{C_j}$

in (12) by W_{ij} and W_{ji} [19].

The spatial discretization (11) has been presented together with a first order scheme in time but it is important to have a precise time integration scheme. In this paper, a low-storage four step Runge-Kutta scheme has been used. Let us rewrite (9) as

$$\frac{\partial W}{\partial t} = RHS(W),$$

where RHS contains the nonlinear operators. The Runge-Kutta scheme we use is given by:

$$W^0 = W^n \,,$$

$$W^k = W^0 + \alpha_k \Delta t \, RHS(W^{k-1}) \quad \text{for} \quad k = 1, .., 4 \,,$$

$$W^{n+1} = W^4 \,,$$

with the following choices for α_k:

$$\alpha_1 = 0.11, \ \alpha_2 = 0.2766, \ \alpha_3 = 0.5, \ \alpha_4 = 1.0 \,.$$

More details can be found in [20].

5 Wall-Laws

The first level in the modeling for wall-laws is to consider attached flows (i.e. without separations) on adiabatic walls (i.e. $\partial_y T \mid_0 = 0$). We are looking for laws valid up to the wall. This means that we would like to include as much as possible the physic represented by a low-Reynolds turbulence model. We consider the following approximated momentum equation in near-wall regions (x and y denote the local tangential and normal directions):

$$\frac{\partial}{\partial y}\left((\mu + \mu_t)\frac{\partial u}{\partial y} \right) = 0, \tag{13}$$

with

$$\mu_t = \kappa\sqrt{\rho\rho_w}\,y\,u_\tau\,(1 - e^{-y^+/70}) \text{ and } y^+ = \frac{\rho_w u_\tau y}{\mu_w}. \tag{14}$$

The equation (13) means that the shear stress along n is constant. u_τ is a constant called the friction velocity and is defined by:

$$u_\tau = (\frac{\mu + \mu_t}{\rho_w}\frac{\partial u}{\partial y})^{1/2}, \tag{15}$$

where w means at the wall.

5.1 High-Reynolds regions

In high-Reynolds regions, the eddy viscosity becomes $\mu_t = \kappa\sqrt{\rho\rho_w}yu_\tau$ and dominates the laminar one; this point leads to the logarithmic law:

$$\frac{\partial u}{\partial y} = \frac{u_\tau}{\kappa y}\sqrt{\frac{\rho_w}{\rho}},\ u = u_\tau\sqrt{\frac{\rho_w}{\rho}}(\frac{1}{\kappa}\,\log(y) + C),$$

provided that $\partial_y \rho \ll \partial_y u$. This hypothesis is realistic because $\partial_y p \sim 0$ and $\partial_y T = 0$, as the wall is adiabatic. Therefore, $\partial_y \rho \sim 0$. At this level, the presence of the Reynolds number is implicit in the constant C. To have a universal expression, we write:

$$u = u_\tau \sqrt{\frac{\rho_w}{\rho}}(\frac{1}{\kappa} \log(y^+) + \beta),$$

where $\beta = -\dfrac{1}{\kappa} \log(\dfrac{u_\tau \rho_w}{\mu_w}) + C$ is found to have a universal value of 5 for incompressible flows.

5.2   Low-Reynolds regions

In low Reynolds regions, μ_t is neglected in (13) which leads to a linear behavior for u vanishing at walls:

$$\rho_w u_\tau^2 = \mu \frac{\partial u}{\partial y} \sim \frac{\mu u}{y}.$$

This means that:

$$u^+ = \frac{u}{u_\tau} = \frac{y u_\tau \rho_w}{\mu_w} = y^+.$$

5.3   General expression

To have a general expression, we define the friction velocity u_τ, solution of

$$u = u_\tau \sqrt{\frac{\rho_w}{\rho}} f(u_\tau), \tag{16}$$

where f is such that $w = u_\tau \sqrt{\frac{\rho_w}{\rho}} f(u_\tau)$ is solution of (13-14). The wall-function therefore is not known explicitly and depends on density distribution. Unfortunately, it is not easy to solve this system for both low and high Reynolds regions. We make the choice to propose a hierarchie of laws taking into account compressibility effects starting from low-speed laws.

For low-speed flows, where density variations are supposed negligible, a satisfactory choice for f is the nonlinear Reichardt function f_r defined by:

$$f_r(y^+) = 2.5 \log(1 + \kappa y^+) + 7.8\left(1 - e^{\frac{-y^+}{11}} - \frac{y^+}{11} e^{-0.33 y^+}\right), \quad \text{with} \quad y^+ = \frac{y u_\tau \rho_w}{\mu_w}. \tag{17}$$

This expression fits both the logarithmic and the linear velocity profiles. In what follows, we will try to find extensions for this law for high-speed flows.

6 Corrections for adiabatic walls for compressible flows

Note that the previous wall-laws are valid for incompressible flows. We need to introduce therefore some corrections to take into account the compressible feature of the flow. By now, ∞ will denote inflow quantities and e will refer to the nearest local value outside boundary layer. We need to account for density variation in (16) and for the fact that Reichardt law has been suggested for low-speed flows.

6.1 Prescribing ρ_w

Let us define the recovery factor [21]:

$$ r = \frac{T_f - T_e}{T_{ie} - T_e}, $$

where T_f is called the friction temperature and T_{ie} is given by:

$$ T_{ie} = T_e \, (1 + \frac{\gamma - 1}{2} M_e^2). $$

For turbulent flows, it is admitted that $r = Pr^{1/3}$ [21]. We obtain

$$ T_f = T_e \, (1 + Pr^{\frac{1}{3}} \frac{\gamma - 1}{2} M_e^2). $$

In the adiabatic case, the wall temperature is the friction temperature T_f [21] (i.e. $T_w = T_f$).

To close (14) in the adiabatic compressible case, we have to provide μ_w and ρ_w. The viscosity at the wall μ_w is obtained thanks to the Sutherland law:

$$ \mu_w = \mu_e \, (\frac{T_w}{T_e})^{1/2} \, \frac{1 + 110.4/T_e}{1 + 110.4/T_w} \, . \tag{18} $$

For the second quantity, we use the Crocco relation [21].
Crocco's law expresses that:

$$ T = T_w + (T_{ie} - T_w) \frac{u}{u_e} - (T_{ie} - T_e) \, (\frac{u}{u_e})^2 \, , $$

As a consequence, we have:

$$ \frac{T}{T_w} = 1 + [(1 + \frac{\gamma - 1}{2} M_e^2) \frac{T_e}{T_w} - 1] \frac{u}{u_e} - \frac{\gamma - 1}{2} M_e^2 \frac{T_e}{T_w} \left(\frac{u}{u_e} \right)^2 \, . $$

We suppose the static pressure constant in the normal direction (i.e. $\partial_y p = 0$), therefore, from the perfect gas law, we obtain:

$$\frac{\rho_w}{\rho} = \frac{T}{T_w} \, .$$

So, we evaluate ρ_w thanks to:

$$\rho_w = \rho \left(1 + [(1 + \frac{\gamma - 1}{2} M_e^2)\frac{T_e}{T_w} - 1]\frac{u}{u_e} - \frac{\gamma - 1}{2}M_e^2\frac{T_e}{T_w}\left(\frac{u}{u_e}\right)^2 \right) \, . \qquad (19)$$

Remark:

The implementation of (18) and (19) is not straightforward on unstructured meshes as it is difficult to determinate (u_e, T_e, M_e). We therefore choose to use only quantities known for any unstructured meshes: at the 'fictitious' wall or at inflow. In particular, M_e is replaced by $M_\delta = \sqrt{\frac{u^2+v^2}{\frac{\gamma P}{\rho}}}$. More precisely, knowing $(\rho_\delta, T_\delta, M_\delta, u_\infty, T_w)$ we find ρ_w by:

$$\rho_w = \rho_\delta \left(1 + [(1 + \frac{\gamma - 1}{2} M_\delta^2)\frac{T_\delta}{T_w} - 1]\frac{u_\delta}{u_\infty} - \frac{\gamma - 1}{2}M_\delta^2\frac{T_\delta}{T_w}\left(\frac{u_\delta}{u_\infty}\right)^2 \right) \, . \qquad (20)$$

This expression therefore uses only local informations at the wall.

6.2   Correction for Reichardt law

The next step is to introduce a correction for the Reichardt law. Three approaches have been tested.

A -   Following Cousteix [21], we express the turbulent tension thanks to the mixing-length formula for high-Reynolds region ($\kappa y \partial_y u = u_\tau$):

$$\rho_w u_\tau^2 = \rho \kappa^2 y^2 (\partial_y u)^2 \, ,$$

so that:

$$\frac{\partial u}{\partial y} = \sqrt{\frac{\rho_w}{\rho}} \frac{u_\tau}{\kappa y}.$$

We express ρ_w/ρ thanks to the Crocco law and obtain:

$$\frac{\partial u}{\partial y} = \frac{u_\tau}{\kappa y}\left(1 + b\frac{u}{u_\infty} - a^2\left(\frac{u}{u_\infty}\right)^2\right) \, , \qquad (21)$$

with $a^2 = \dfrac{\gamma - 1}{2}\, M_\delta^2\, \dfrac{T_\delta}{T_w}$ and $b = (1 + \dfrac{\gamma - 1}{2}\, M_\delta^2)\, \dfrac{T_\delta}{T_w} - 1$.   The weakness of this approach is that it is not valid up to the wall. A global correction needs a global mixing

length formula as starting point using (16):

$$\frac{\partial u}{\partial y} = u_\tau (\partial_y f(y^+) \sqrt{\frac{\rho_w}{\rho}} + f(y^+) \partial_y (\sqrt{\frac{\rho_w}{\rho}})), \tag{22}$$

which is hardly computable.

B - To avoid the difficulty above, we would like to restart from (13-14):

$$\left(\mu + \sqrt{\rho \rho_w} \kappa u_\tau y (1 - e^{-y^+/70}) \right) \frac{\partial u}{\partial y} = \rho_w u_\tau^2. \tag{23}$$

Now, suppose that the Reichardt law is obtained after integration of:

$$u_\tau = \frac{\partial u}{\partial y} \left(\mu + \kappa y (1 - e^{-y^+/70}) \right). \tag{24}$$

First consider the case $y^+ > 100$ and drop the laminar viscosity. Hence, replacing u_τ by (24) in the left hand side of (23), leads to:

$$\frac{\partial u}{\partial y} = \sqrt[4]{\frac{\rho_w}{\rho}} \frac{u_\tau}{\kappa y (1 - e^{-y^+/70})}. \tag{25}$$

The Crocco law links density and temperature and (25) becomes:

$$\frac{\partial u}{\partial y} = \sqrt[4]{1 + b\frac{u}{u_\infty} - a^2 \left(\frac{u}{u_\infty} \right)^2} \frac{u_\tau}{\kappa y (1 - e^{-y^+/70})}, \tag{26}$$

The integration of relation (26) is not possible. At this level, we use the following approximation:

$$\left(\frac{1}{a}(\arcsin \frac{2\,a^2\,u/u_\infty - b}{\sqrt{b^2 + 4\,a^2}} + \arcsin \frac{b}{(b^2 + 4\,a^2)^{1/2}}) \right)^{1/2} = u_\tau\, f_r(y^+).$$

If laminar viscosity dominates the eddy one $(y^+ < 20)$,

$$\rho_w u_\tau^2 = \mu \frac{\partial u}{\partial y}. \tag{27}$$

For $20 < y^+ < 100$, we use a linear interpolation between the two expressions above.

Remark:

This formula gives the best results for the numerical simulations and is valid up to the wall.

C - Another way to proceed is due to Van Driest [21, 22], considering the log law relation as starting point in (24), this leads to a relation only valid for high Reynolds region. But experience shows that it does not extend well up to the wall.

6.3 Energy equation

Consider the viscous part of the energy equation written in the boundary layer (i.e. $\partial_x << \partial_y$):

$$\frac{\partial}{\partial y}(u(\mu + \mu_t)\frac{\partial u}{\partial y}) + \frac{\partial}{\partial y}((\chi + \chi_t)\frac{\partial T}{\partial y}) = 0.$$

When we integrate this equation between the fictitious wall ($y = \delta$) and the real one ($y = 0$), we obtain:

$$(\chi + \chi_t)\frac{\partial T}{\partial y} \mid_\delta -\chi\frac{\partial T}{\partial y} \mid_0 = u(\mu + \mu_t)\frac{\partial u}{\partial y} \mid_0 -u(\mu + \mu_t)\frac{\partial u}{\partial y} \mid_\delta . \tag{28}$$

So, thanks to $\partial_y T \mid_0 = 0$ and $u \mid_0 = 0$:

$$(\chi + \chi_t)\frac{\partial T}{\partial y} \mid_\delta +u(\mu + \mu_t)\frac{\partial u}{\partial y} \mid_\delta = 0.$$

Therefore, in the adiabatic case, there is no term for the energy equation to account for.

7 Isothermal walls

7.1 The Reynolds relation

For isothermal walls ($T_w = T_{given}$), we have to provide a law for the temperature, as we did for the velocity. In weak form, we only need a law for the thermal stress $\chi \partial_y T$. A first attempt is to use the classical Reynolds relation between heat and friction coefficients [21]:

$$C_h = \frac{s\,C_f}{2} = \frac{1.24}{2}C_f = 0.62C_f.$$

So, we have:

$$-\frac{\chi\partial_y T}{\rho u^3\gamma} = C_h = 0.62C_f = 1.24\frac{\rho_w u_\tau^2}{\rho u^2},$$

Note that, for the isothermal case, as $(\mu + \mu_t)\partial_y u = \rho_w u_\tau^2$, (28) leads to:

$$(\chi + \chi_t)\frac{\partial T}{\partial y} \mid_\delta +u\rho_w u_\tau^2 = \chi\frac{\partial T}{\partial y} \mid_0 .$$

So, we have:

$$(\chi + \chi_t)\frac{\partial T}{\partial y} \mid_\delta +u\rho_w u_\tau^2 = -1.24\rho_w u_\tau^2\gamma u. \tag{29}$$

Here, the definition of the friction and heat coefficients are based on local values. The wall density is obtained through the Crocco law.

7.2 Crocco's method

Instead of using the Reynolds relation between heat and friction coefficients, as the only term that we have to evaluate is $\partial_y T$, we can obtain this gradient from Crocco's law:

$$\frac{T}{T_w} = 1 + [(1 + \frac{\gamma - 1}{2} M_\delta^2) \frac{T_\delta}{T_w} - 1] \frac{u}{u_\infty} - \frac{\gamma - 1}{2} M_\delta^2 \frac{T_\delta}{T_w} \left(\frac{u}{u_\infty}\right)^2 .$$

Using $u(y = 0) = 0$, we have:

$$\frac{\partial T}{\partial y} \Big|_0 = \left(T_\delta + \frac{\gamma - 1}{2} M_\delta^2 T_\delta - T_w\right) \frac{\partial}{\partial y}(\frac{u}{u_\infty}) \Big|_0$$

so:

$$\chi \frac{\partial T}{\partial y} \Big|_0 = \frac{\chi}{\mu} \left(T_\delta + \frac{\gamma - 1}{2} M_\delta^2 T_\delta - T_w\right) \rho_w u_\tau^2 . \tag{30}$$

Moreover, we can assume that the modelisation is not achieved because it is obvious that in the recirculation areas, the friction velocity u_τ is small (and u also). As a consequence, the prediction of the boundary condition for the energy equation will be too small in these areas. As a matter of fact, we will have to change the previous relations (29,30) in areas with recirculation.

7.3 The recirculation areas

The problem with separation and recirculation areas comes from the fact that the variables u and u_τ needed by our wall-laws are very small. As a consequence, this leads to an underestimation of the heat flux. So, we have to define another expression to replace $\rho_w u_\tau^2 = (\mu + \mu_t)\partial_y u$ in relations (29) and (30). One issue is to change the velocity scale. By a dimension argument, we choose the local velocity scale to be $u = c_\mu^{-3/4}\sqrt{k}$.

Hence, the friction flux is given by:

$$(\mu + \mu_t)\frac{\partial u}{\partial y} = c_\mu^{-3/4}(\mu + \mu_t)\frac{\partial \sqrt{k}}{\partial y} . \tag{31}$$

8 k and ε boundary conditions at the fictitious wall

Once u_τ is computed, k and ε are set to:

$$k = \frac{u_\tau^2}{\sqrt{c_\mu}}\alpha , \quad \varepsilon = \frac{k^{\frac{3}{2}}}{l_\varepsilon} ,$$

where $\alpha = min(1, (\frac{y^+}{10})^2)$ reproduces the behavior of k when δ tends to zero (δ is the distance of the fictitious computational domain from the solid wall). The distance δ is given a priori and is kept constant during the computation. l_ε is given by (8).

9   Wall-Laws Implementation

We define $\mathbf{S} = (\mu + \mu_t)(\nabla u + \nabla u^t - \frac{2}{3}\nabla.uI)$ and $(\vec{t}, \vec{n})$ as the local orthogonal basis for a wall node. In weak form (finite element or finite volume approaches),

$$\int_{\Gamma_w} (\mathbf{S}.\vec{n})d\sigma$$

appears in the momentum equation and

$$\int_{\Gamma_w} \left((u\mathbf{S}.\vec{n}) + (\chi + \chi_t)\nabla T.n\right)d\sigma$$

appears in the energy equation . This former quantity vanishes in the adiabatic case as seen above and for the isothermal case, it reduces to:

$$\int_{\Gamma_w} -1.24\rho_w \frac{T_w - T_f}{u}(\mu + \mu_t)\frac{\partial u}{\partial n}\,d\sigma \text{ using the Reynolds relation,}$$

or to

$$\int_{\Gamma_w} \left(\frac{\chi}{\mu}(\frac{\gamma - 1}{2}M^2 T + T - T_w)\right)(\mu + \mu_t)\frac{\partial u}{\partial n}\,d\sigma \text{ using the Crocco method.}$$

10   Numerical Experiments

This section is devoted to the validation of these wall functions for unstructured meshes for separated hypersonic flows over expansion and compression ramps and for a supersonic flow on a circular cylinder.

10.1   The adiabatic expansion ramp

We consider an adiabatic expansion ramp at $M_\infty = 4$ and $Re_\infty = 4.5\ 10^7$. We use a 1D boundary layer code to generate the inflow profiles for all the variables for a boundary layer corresponding to $Re_{\delta_0} = 1.7\ 10^5$ (see appendix 1). The angle of the ramp is -25 degrees [23]. The mesh used has about 6000 nodes with the first point in the normal direction at $7\ 10^{-5}m$ from the wall. The wall is considered as adiabatic. The flow configuration is shown in figure (1). The pressure distribution agrees well with experimental values available in [23] (see figure (2)). The friction coefficient prediction (figure 3) has been improved using our compressibility corrections, without them and with a correction extracted from (22). In fact, these results improve our compressibility modifications based on local informations at the fictitious wall. The results presented in [23, 24] show a lower estimation of the skin friction coefficient using $k - \varepsilon$, $q - \omega$ and

various two-layer models, than the present. In addition to this satisfactory predicting level, we notice also that the recirculation has been captured despite the fact that it is only driven by pressure effects and not the geometry. This is coherent with our previous observations about the ability of wall-laws in capturing complex separations [2, 3].

10.2 The adiabatic circular cylinder

We consider the flow over the upper left quarter of an adiabatic circular cylinder which diameter is $1m$. The inflow Mach number is 2 and the Reynolds one is 10^7. Moreover, the inflow fluid temperature is $161K$. The aim of this study is to test the validity of our wall-laws on curve walls. As we did not have any experimental data, the results evaluated thanks to the two-layer $k - \varepsilon$ model (8) will give us reference quantities.

We have used three meshes: one with first nodes in the normal direction at $3.\,10^{-5}m$ from the wall is used for wall-laws computations, a refined mesh with first node at $1.\,10^{-5}m$ from the wall demonstrates the mesh-independence of the results, while the third one, with the first nodes in the normal direction at $1.\,10^{-6}m$ from the wall, is used for two-layer computations.
The CPU cost is much more lower with wall-laws as the mesh is coarser and time steps higher (by three orders of magnitude here).

Figures (5) show a good agreement for the behavior of the velocity at the 135 degrees cross-section with both the methods. The results obtained with our wall-laws for the temperature at this cross-section have the same property (figures 6). The turbulent kinetic energy behavior is the same with wall-laws and the two-layer model (figure 7). So, the good agreement of the results obtained with the different method validate our wall-laws on curve walls.

10.3 The isothermal compression ramp

We consider the isothermal Delery 35 degrees compression ramp presented at Hermes Workshop [25]. Experimental results are available for the pressure and heat flux distributions. The inflow Mach and Reynolds numbers are respectively 5 and 4.10^7. The mesh used has about 8000 nodes and the first point in the normal direction is at a distance of $5.\,10^{-6}m$ from the wall, the corner being at $0.25m$ from the leading edge. The inflow temperature is $T_\infty = 83K$ and the wall temperature $T_{wall} = 288K$. The pressure coefficient distribution agrees with experimental results, with some overestimation in the plateau region (figure 9). We use the formulation presented in (29) to evaluate the heat flux (figure 10). The effects of our post-processing formula (29) compared to the heat contribution alone (i.e. $(\chi + \chi_t)\partial_y T/(\rho u^3 \gamma)$) are shown in figure (11). We can see a correct behavior in the flat region and a better fit with experience after separation. As we have said, a good fit with the experimental data in the recirculation areas was

impossible with either formulation (29) or (30) because of the speeds u and u_τ too much small. In figures (13) and (12), we present the results obtained with the formulation (31) and the fit with experimental data is better for the heat transfer coefficient. As before, the recirculation length is under-predicted.

We present on figure (14) the heat transfer coefficient obtained thanks to the two layer model. For this case, a refined mesh has been used : more than 14000 nodes, and with the first ones in the normal direction at less than $2.10^{-7}m$ from the real wall. This figure shows that the behavior are the same using wall-laws with coarse meshes or using the two-layer $k - \varepsilon$ model with very refined meshes near the real wall. Moreover, figures (12) and (14) shows that the fit with experimental data is better on attached with wall-laws than with the two-layer technique. Furthermore, as when wall-laws are applied, the recirculation length is under estimated and the numerical error is the same. So, the error in predicting the recirculation length is not a problem of wall-laws, but a problem of modelisation.

As a consequence, this is a numerical validation of our thermal wall-laws.

11   Concluding remarks

The application of a new wall-laws formulation for compressible flows over adiabatic and isothermal walls has been shown. This approach is general in the sense that the laws are valid up to the wall (for all y^+), for a wide range of Mach number and heat flux distribution over the wall. The work has been motivated by an industrial demand for general laws on 3D unstructured type meshes for complex geometries. This is why only local informations available at the fictitious wall nodes have been used. Hence, the extension to 3D is straightforward. We showed that separated flows can be computed on relatively coarse meshes using explicit schemes. One advantage of this approach is the fact that due to the weak formulation, it is not necessary to provide a global law for the temperature, while a global law was necessary for the velocity. It is well known that this is quite difficult because of the complex shape of the temperature boundary layer. Our current effort is therefore to improve our relation for the heat flux definition and to extend these laws to rough boundaries.
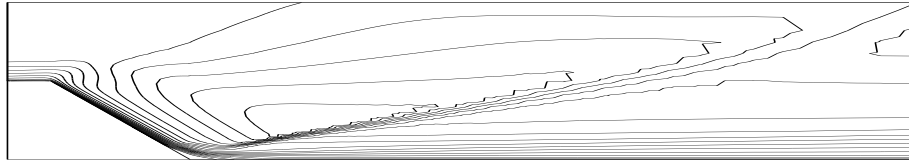
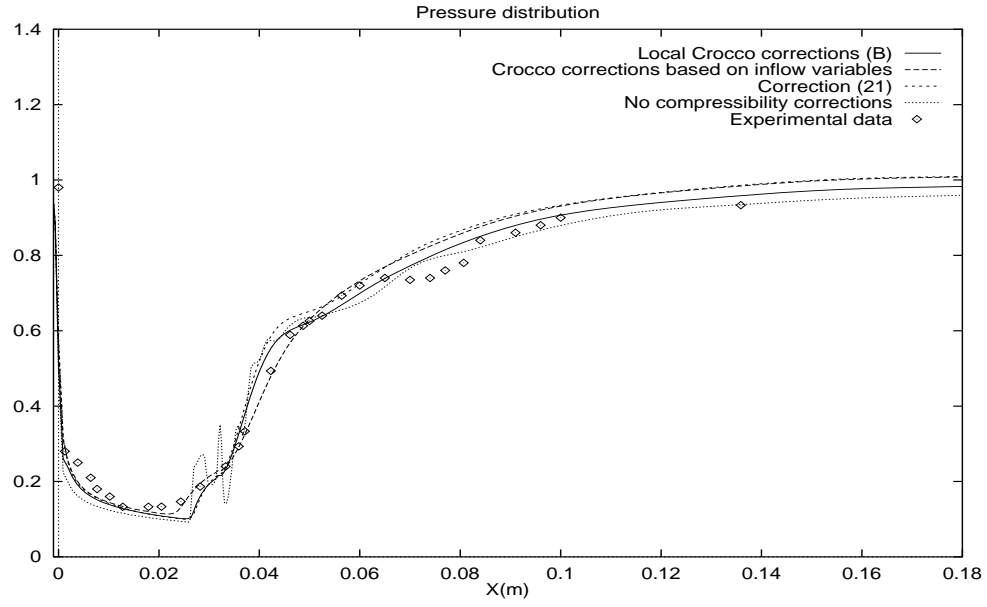Figure 1: *Adiabatic expansion ramp ($M_\infty = 4$, $Re_\infty = 45.10^6$): iso-Mach contours.*

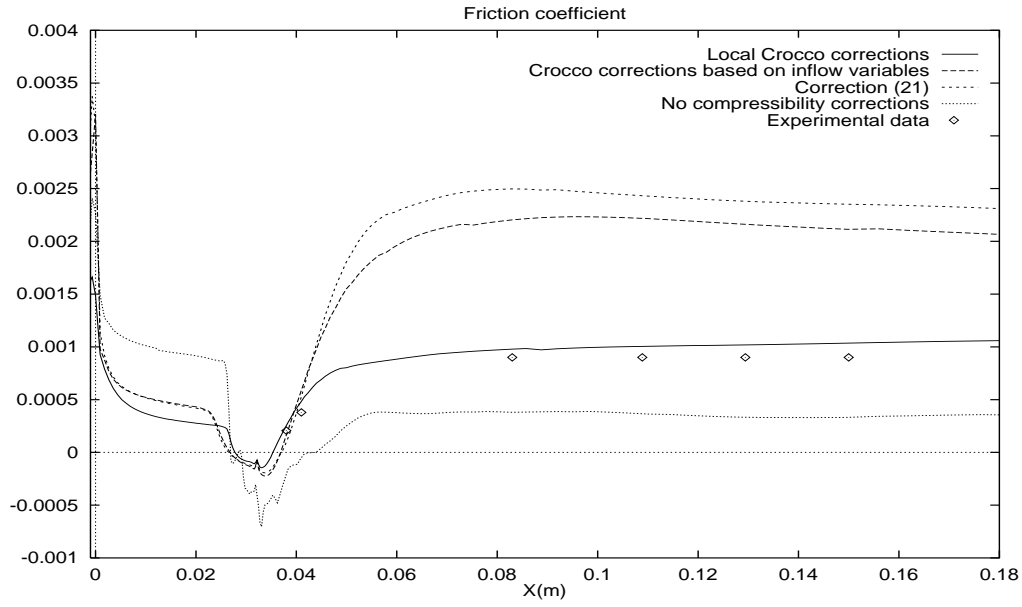Figure 2: *Adiabatic expansion ramp ($M_\infty = 4$, $Re_\infty = 45.10^6$): pressure distribution.*

Figure 3: *Adiabatic expansion ramp ($M_\infty = 4$, $Re_\infty = 45.10^6$): friction coefficient, effects of the compressibility corrections. The best agreement is obtained with correction (20).*
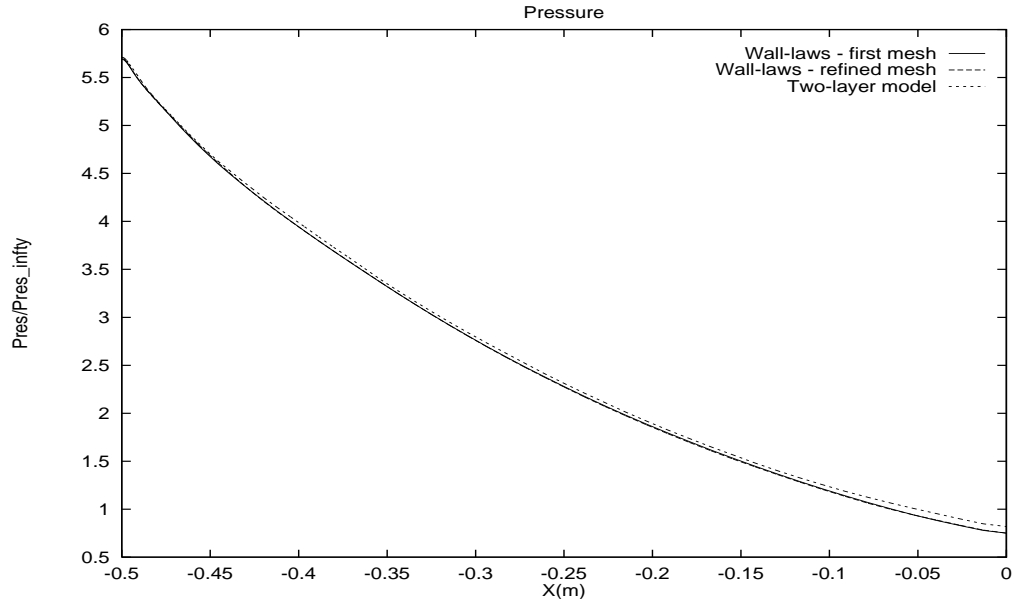

Figure 4: *Flow over the upper left quarter of an adiabatic circular cylinder: wall pressure distribution with wall-laws or with the two-layer model.*
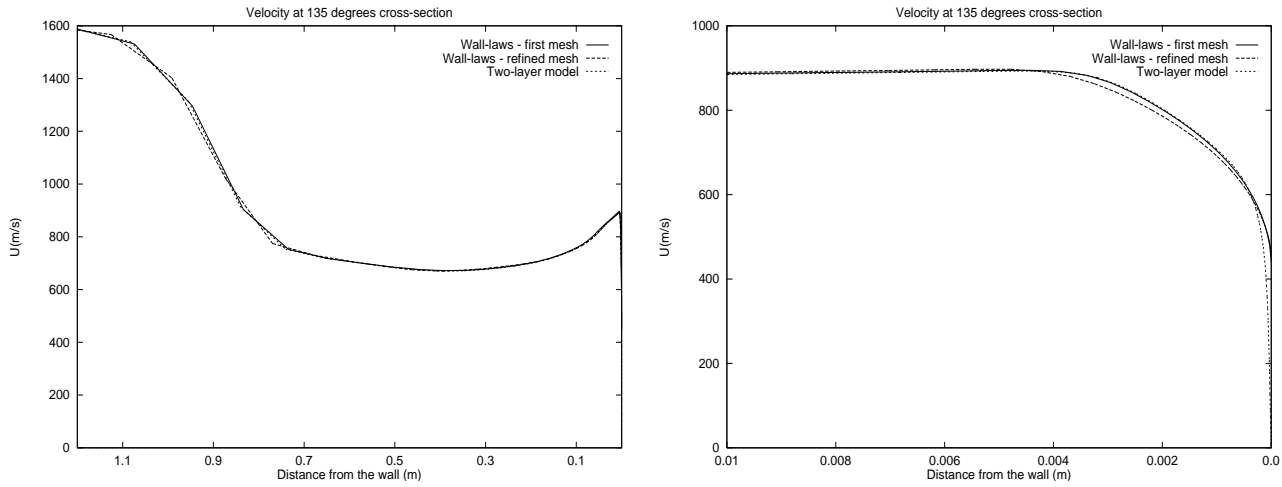
Figure 5: *Adiabatic circular cylinder: velocity of the fluid at the 135 degrees cross-section evaluated with our wall-laws or with the two-layer model.*
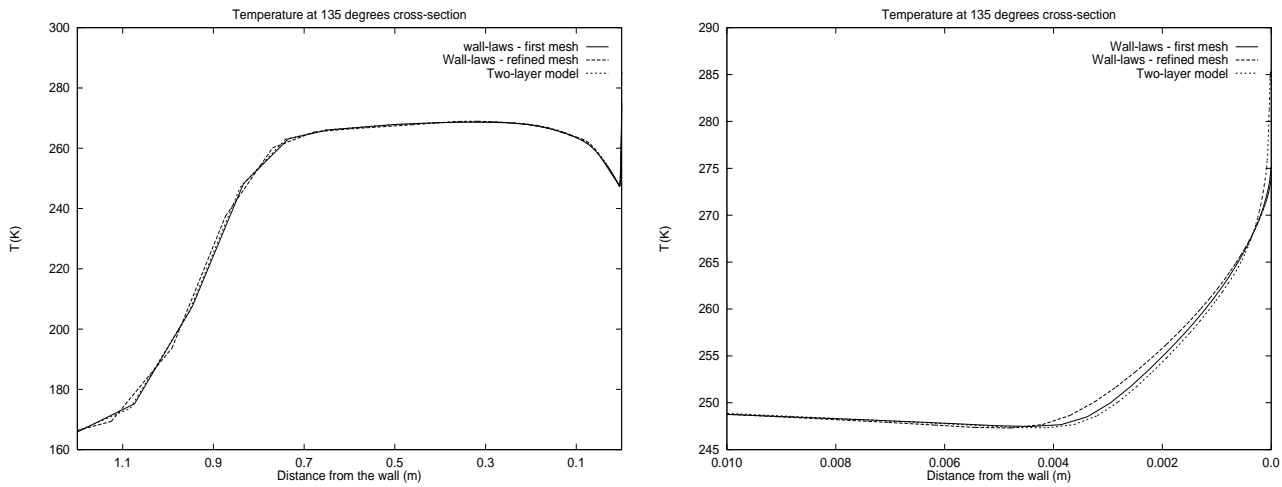
Figure 6: *Adiabatic circular cylinder: temperature of the fluid at the 135 degrees cross-section evaluated with our wall-laws or with the two-layer model.*
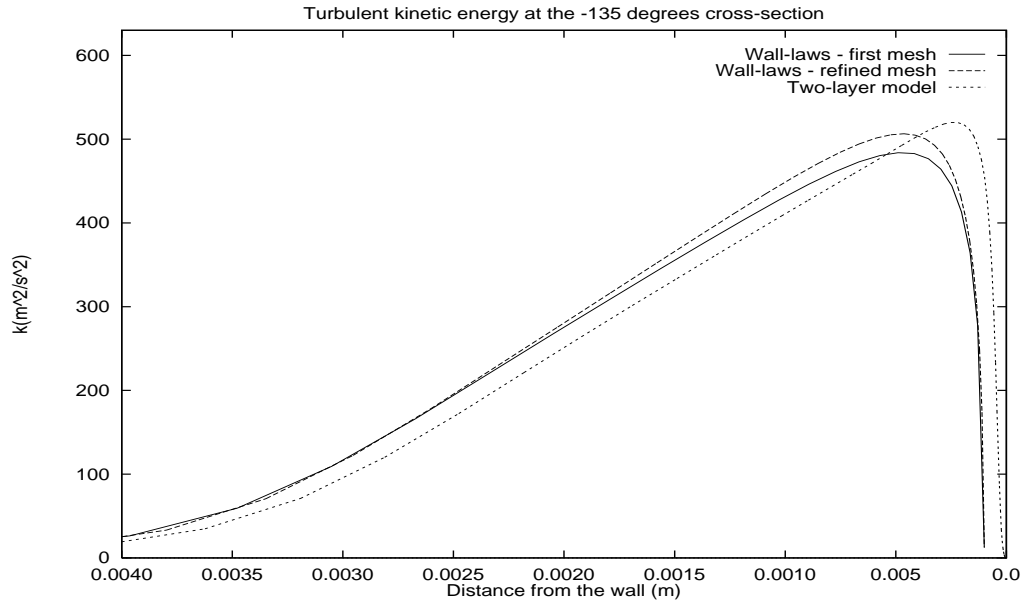
Figure 7: *Adiabatic circular cylinder: turbulent kinetic energy at the 135 degrees cross-section near the wall.*
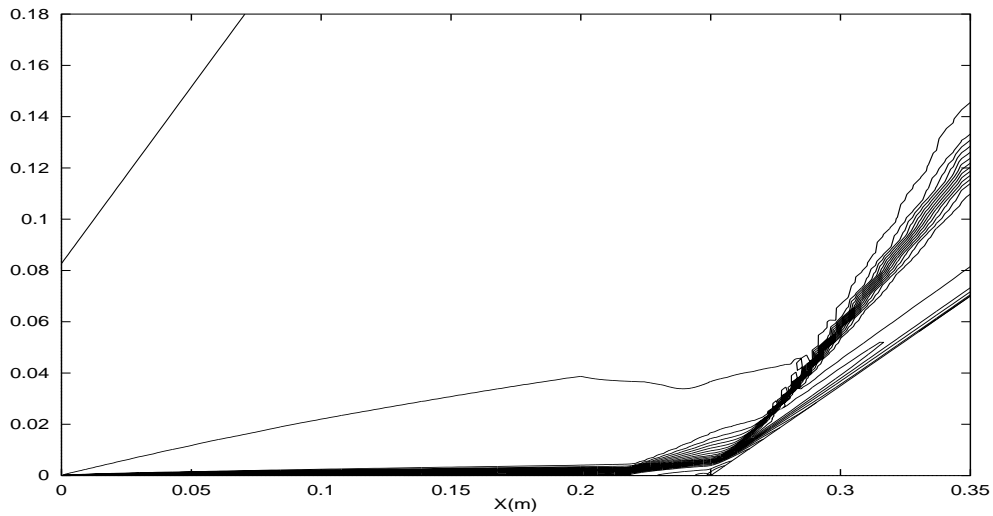
Figure 8: *Isothermal compression ramp ($M_\infty = 5$, $Re_\infty = 4.10^7$): magnified view of iso-Mach contours.*
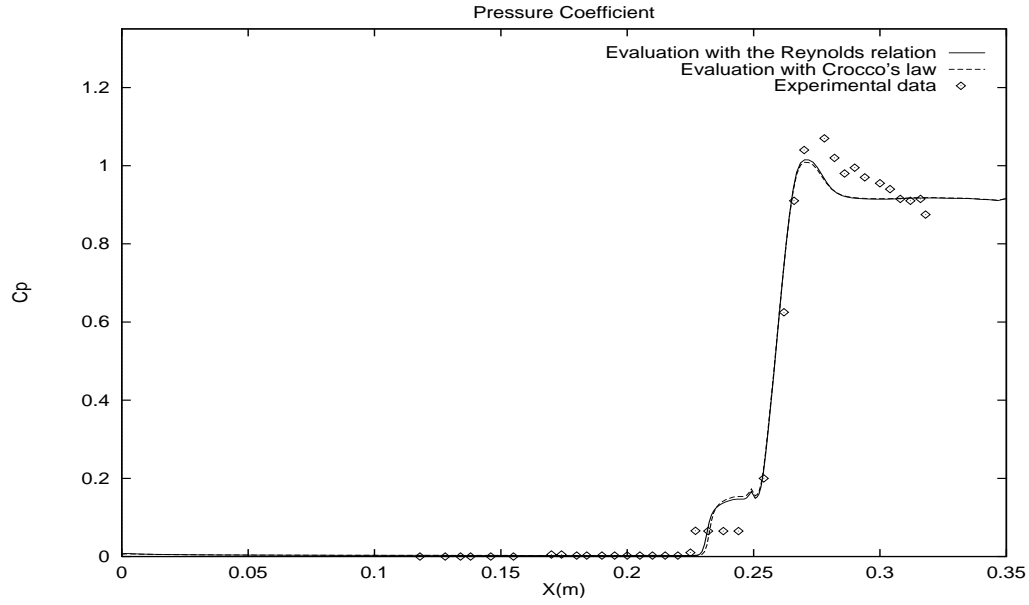
Figure 9: *Isothermal compression ramp ($M_\infty = 5$, $Re_\infty = 4.10^7$, $T_{wall} = 288K$ and $T_\infty = 83K$): pressure coefficient distribution - Reynolds relation against Crocco's law.*
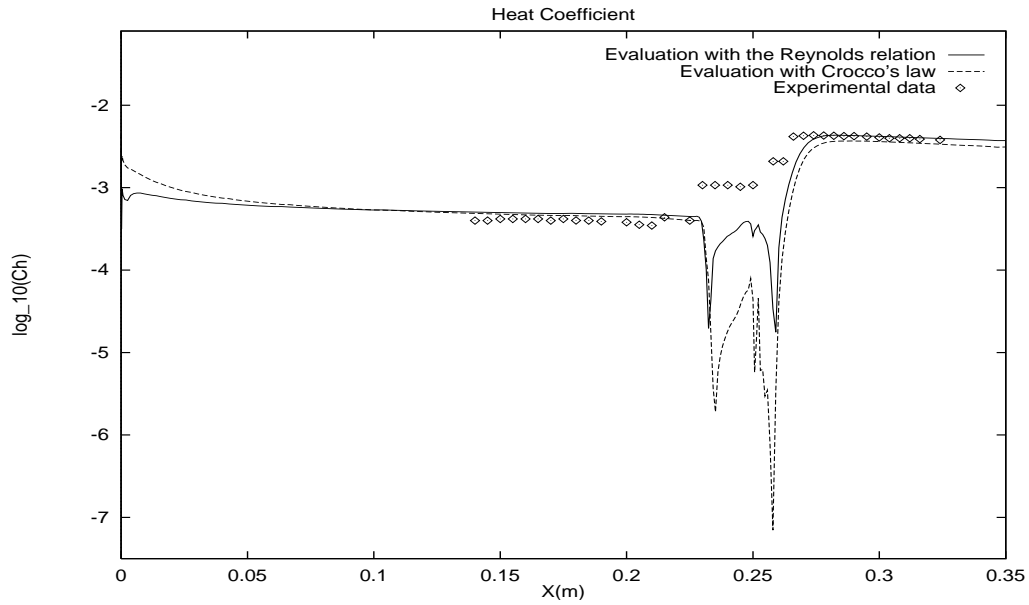

Figure 10: *Isothermal compression ramp ($M_\infty = 5$, $Re_\infty = 4.10^7$, $T_{wall} = 288K$ and $T_\infty = 83K$): heat coefficient distribution - Reynolds relation against Crocco's law.*
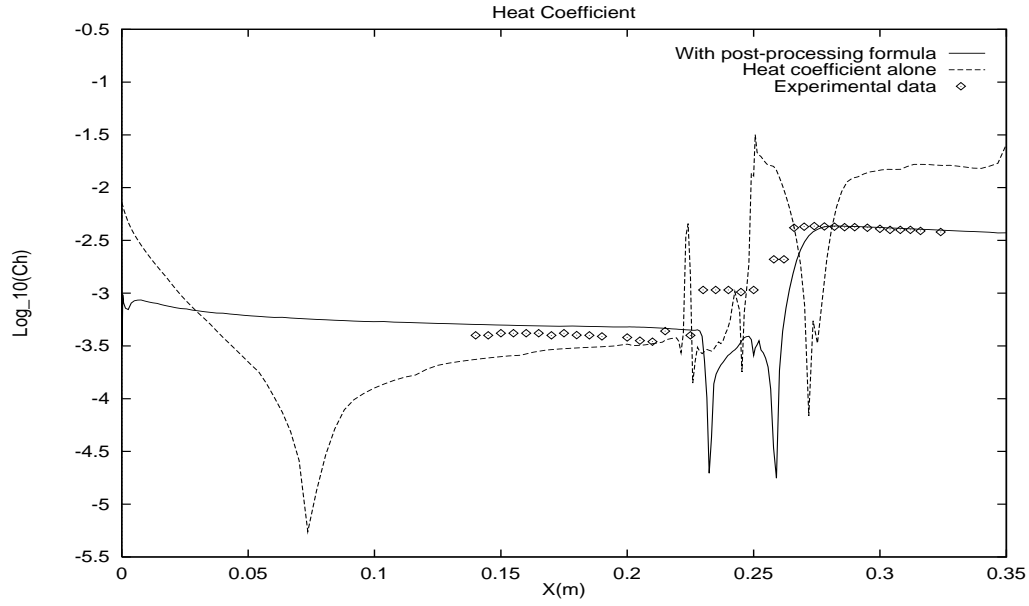
Figure 11: *Isothermal compression ramp* ($M_\infty = 5$, $Re_\infty = 4.10^7$, $T_{wall} = 288K$ *and* $T_\infty = 83K$): *heat coefficient obtained with the Reynolds relation before and after the post processing formula implementation.*
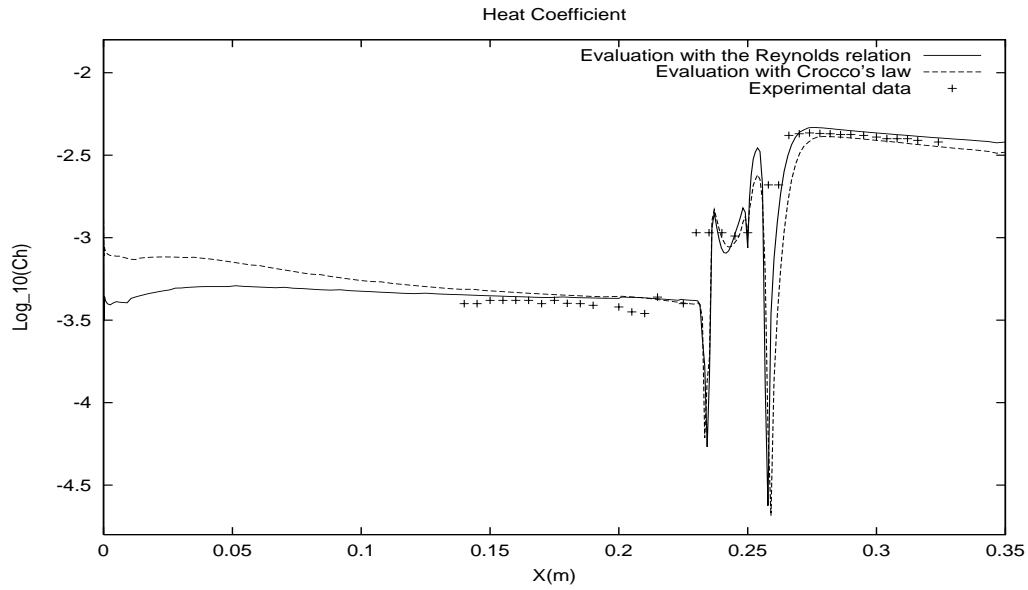

Figure 12: *Isothermal compression ramp* ($M_\infty = 5$, $Re_\infty = 4.10^7$, $T_{wall} = 288K$ *and* $T_\infty = 83K$): *heat coefficient after the implementation of the modifications for the recirculating regions.*
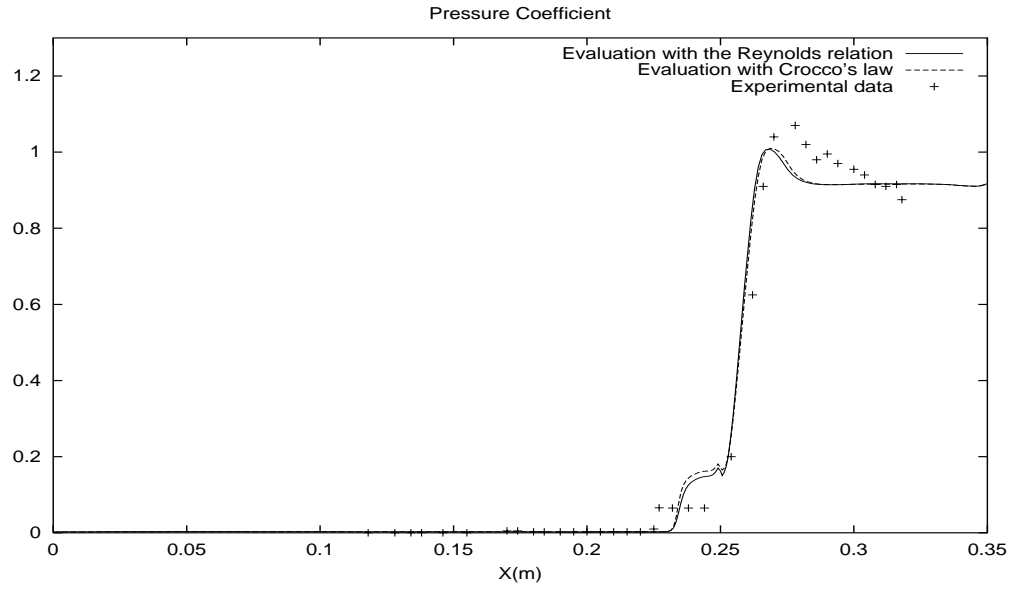
Figure 13: *Isothermal compression ramp ($M_\infty = 5$, $Re_\infty = 4.10^7$, $T_{wall} = 288K$ and $T_\infty = 83K$): pressure coefficient after the implementation of the modifications for the recirculating regions.*
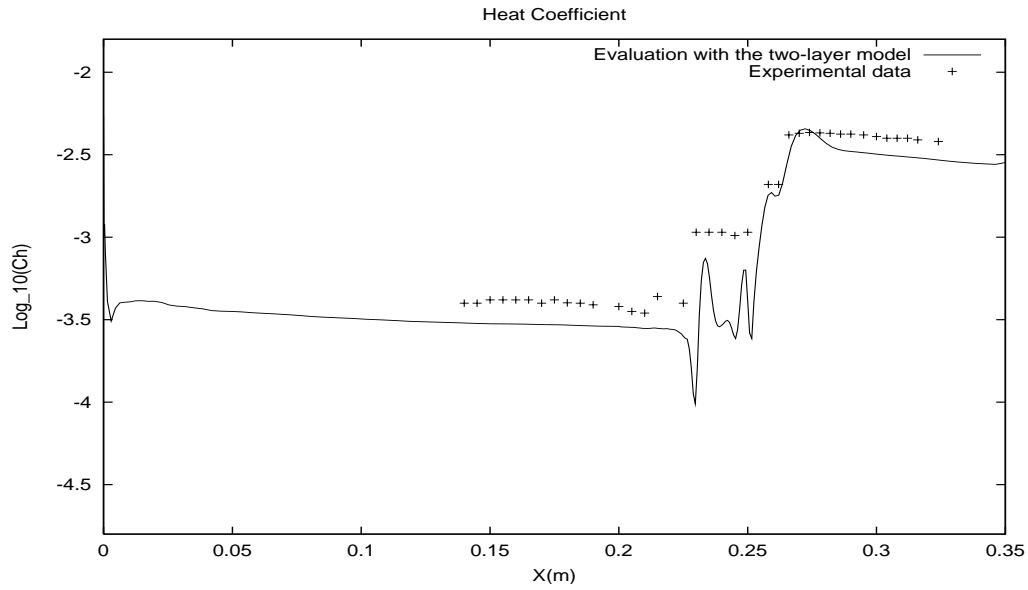

Figure 14: *Isothermal compression ramp ($M_\infty = 5$, $Re_\infty = 4.10^7$, $T_{wall} = 288K$ and $T_\infty = 83K$): heat coefficient obtained thanks to the $k - \varepsilon$ two-layer model.*

12   Appendix 1: Generating Inflow Profiles

We have used a 1D boundary layer code to generate the inflow profiles of the variables for adiabatic cases from the inflow Reynolds number, the inflow Mach number and the inflow fluid temperature and the boundary momentum thickness (θ). The iterative process [26] is as follows:

- *step 0:* R_e, M, T, θ known

- *step 1:* definition of y^+ for each node

- *step 2:* evaluation of u_b^+ from:

$$\frac{\partial u_b^+}{\partial y^+} = \frac{2}{1 + \sqrt{1 + 4\kappa y^+(1. - e^{-y^+/25.53})}} \, .$$

- *step 3:* evaluation of u_c^+ from:

$$u_c^+ = u_b^+ + 0.55(1. - exp(-0.24\sqrt{Re_\theta} - 0.298 Re_\theta)) \frac{2. \sin^2\left(\frac{\pi y}{2.\delta}\right)}{\kappa} \, ,$$

and evaluation of u^+ from:

$$u^+ = \frac{\kappa \sin\left(\frac{u_\tau}{\kappa} u_c^+\right)}{u_\tau} \, .$$

- *step 4:* evaluation of the velocity u, of the temperature T and of the density ρ at each node.

- *step 5:* new definition of the friction velocity u_τ and of the friction coefficient C_f:

$$u_\tau = u_{\tau\text{new}} \text{ and } C_f = C_{f\text{new}} \, .$$

- *step 6:* calculation of θ_{int} and δ_{int} where:

$$\theta_{int} = \int_0^\delta \rho u(1. - u) dy \text{ and } \delta_{int} = \int_0^\delta (1. - u) dy \, .$$

- *step 7:* definition of $\delta = \theta/\theta_{inmt}$, $Re_\delta = \rho_w u_\tau \delta/\mu_w$, $\delta_1 = \delta \delta_{int}$, $h_{12} = \delta_1/\theta$.

- *step 8:* if stop condition false, then go to 1.

Knowing u_τ, ρk and $\rho\varepsilon$ are prescribed following the wall-functions approach (8).

$$\rho k = \rho_w u_\tau^2 min(1, (y^+/10)^2), \text{ and } \rho\varepsilon = \rho_w k^{3/2}/(C\, y\, (1. - e^{-y^+/(2\,C)})) \, ,$$

where $C = 0.419 c_\mu^{-3./4.}$.

13   Appendix 2: The Chien $k - \varepsilon$ turbulence model

In this model, the right hand sides of the $k - \varepsilon$ equations (3)-(4) are given by:

$$S_k = \mu_t P - \frac{2}{3}\rho k \nabla . u - \rho \varepsilon - 2.0\mu \frac{k}{y^2} \, ,$$

$$S_\varepsilon = c_1(1 - e^{-c_3 y^+})\rho k P - \frac{2c_1}{3c_\mu}\rho \varepsilon \, \nabla . u - c_2(1.0 - \frac{0.4}{1.8}e^{-R_t^2/36})\rho \frac{\varepsilon^2}{k} - 2.0 e^{-c_4 y^+}\mu \frac{\varepsilon}{y^2} \, ,$$

$$\text{where } R_t = \frac{\rho k^2}{\mu \varepsilon} \, , \text{ and } y^+ = \frac{\sqrt{c_\mu \rho \rho_w k}y}{\mu} \, .$$

Moreover, the eddy viscosity is defined by:

$$\mu_t = c_\mu(1. - e^{-c_3 y^+})\frac{\rho k^2}{\varepsilon} \, .$$

The constants are the same than for the two-layer model. As a consequence, the major differences between the $k - \varepsilon$ models are the new terms in k/y^2 and ε/y^2 and the damping functions linking the constants with y^+ and R_t. The existence of the new term in k/y^2 comes from the isotropic behavior of ε: in the near wall region ($y \to 0$), we have:

$$\varepsilon \sim 2.0\nu \frac{\partial^2 k}{\partial y^2} \sim 2.0\nu \frac{k}{y^2} \, ,$$

so we define $\varepsilon_{isotropic}$ by $\varepsilon_{isotropic} = \varepsilon_{anisotropic} - 2.0\nu \frac{k}{y^2}$. Moreover, these terms need the calculation of the distance between a node and the wall (very difficult to determinate for complex geometries).

References

[1] B. Mohammadi and O. Pironneau (1994),*Analysis of the K-Epsilon Turbulence Model*, WILEY, (Book).

[2] B. Mohammadi and O. Pironneau, (1997) *Unsteady Separated Turbulent Flows Computation with Wall-Laws and $k - \varepsilon$ Model*, CMAME, 148, pp:393-405.

[3] B. Mohammadi and G. Medić, (1998), *A Critical Evaluation of the Classical $k - \varepsilon$ Model and Wall-Laws for Unsteady Flows over Bluff Bodies*, IJCFD, Vol.10, Number 1, pp. 1-12.

[4] V.C. Patel, H.C. Chen (1988), *Near-wall turbulence models for complex flows including separation*, AIAA Journal vol. 29, no. 6.

[5] B. Mohammadi (1992), *Complex Turbulent Compressible Flows Computation with a Two-Layer Approach*, Int. J. Num. Meth. for Fluids, Vol. 15, pp. 747-771.

[6] B.E. Launder and D.B. Spalding (1972),*Mathematical Models of Turbulence,* Academic Press.

[7] B. Mohammadi (1997),*Practical Applications to Fluid Flows of Automatic Differentiation for Design Problems*, VKI lecture motes, LS-05-1997

[8] B. Mohammadi (1999),*Dynamical Approaches and Incomplete Gradients for Shape Optimisation and Flow Control*, VKI lecture motes, American Institute for Aeronautics and Astronautics, num:99-3374

[9] B. Koobus, B. Mohammadi, G. Puigt (1999),*Distributed 3D Shape Optimization with Incomplete Sensitivities and CAD-Frss Framework for High Speed Inviscid and Viscous Turbulent Regimes*, AIAA 2000-4526

[10] G. Dury (1997),*Influence d'une paroi sinusoïdale sur une couche limite en régime supersonique*, Ph.D. Thesis, University of Poitiers

[11] F. Valentin (1998), *Nouvelles conditions aux limites équivalentes pour des interfaces rugueuses en mécanique des fluides : développement, analyse et mise en oeuvre numérique*, Ph.D.Thesis, University Pierre et Marie Curie - Paris VI.

[12] D. Vandromme (1983),*Contribution à la modélisation et à la prédiction d'écoulements turbulents à masse volumique variable,* Ph.D. thesis, University of Lille.

[13] B. Aupoix, E. Desmet, (1992),*Etude de modèles de turbulence en écoulement hypersonique,* report for ONERA/CERT No.48/5005.40

[14] G. Comte-Bellot, S. Corsin (1971), *Simple Eulerian Time-Correlation of Full and Narrow-Band Velocity Signals in Grid-Generated Isotropic Turbulence,* JFM, vol.48, pp:273-33 7.

[15] S. Thangam (1991),*Analysis of Two-Equation Turbulence Models for Recirculating Flows,* ICASE report No. 91-61.

[16] J. Steger, R.F. Warming (1983), *Flux Vector Splitting for the Inviscid gas dynamic with Applications to Finite-Difference Methods,* J. Comp. Phys. 40, pp:263-293.

[17] P.L.Roe (1981), *Approximate Riemann Solvers, Parameters Vectors and Difference Schemes,* J.C.P. Vol.43.

[18] G.D.Van Albada, B. Van Leer (1984),*Flux Vector Splitting and Runge-Kutta Methods for the Euler Equations,* ICASE 84-27.

[19] A. Dervieux (1984),*Steady Euler Simulations using Unstructured Meshes,* VKI lecture series, 1884-04.

[20] B. Mohammadi (1994),*CFD with NSC2KE : an User Guide,* Technical report INRIA No.164.

[21] J. Cousteix (1990),*Turbulence et couche limite,* Ed. Cepadues.

[22] E.R. Van Driest (1951),*Turbulent Boundary Layers in Compressible Fluids,* J. of Aeronautics Science, vol. 18, Num. 145.

[23] A.A. Zheltovodov, V.M. Trofimov, E.Kh. Shilein and V.N. Yakolev (1990), *An Experimental Documentation of Supersonic Turbulent Flows in the Vincinity of Forward- and Backward-facing Ramps,* Report No 2030, Inst. of Theorical and Appl. Mechanics RAS, Novosibirsk .

[24] A.V. Borisov, V.B. Karamishev (1990),*Numerical modeling of separated turbulent flows,* Izv. Sibir. Otdel. Akad Nauk SSSR, Seriya Tekhnicheskikh Nauk, Vol 1, pp:37-43.

[25] J. Delery, M.C. Coet (1990), *Experiments on shock-wave/boundary-layer interactions produced by two-dimensional ramps and three-dimensional obstacles,* Proc. on Workshop on Hypersonic Flows for Reentry Problems, Antibes 22-26, Wiley.

[26] P.G. Huang, P. Bradshaw and T.J. Coakley (1993),*Skin Friction and Velocity Profile Family for Compressible Turbulent Boundary Layers,* A.I.A.A. Journal, vol.31 No 9 pp 1600-1604